

A radio halo surrounding the Brightest Cluster Galaxy in RXCJ0232.2-4420 : a mini-halo in transition ?

Ruta Kale,¹[★] Krishna M. Shende,¹ and Viral Parekh²

¹*National Centre for Radio Astrophysics, Tata Institute of Fundamental Research, S. P. Pune University Campus, Ganeshkhind, Pune 411007, India*

²*Department of Physics and Electronics, Rhodes University, PO Box 94, Grahamstown, 6140, South Africa*

Accepted XXX. Received YYY; in original form ZZZ

ABSTRACT

Diffuse radio sources associated with the intra-cluster medium are direct probes of the cosmic ray electrons and magnetic fields. We report the discovery of a diffuse radio source in the galaxy cluster RXCJ0232.2-4420 (SPT-CL J0232-4421, $z = 0.2836$) using 606 MHz observations with the Giant Metrewave Radio Telescope. The diffuse radio source surrounds the Brightest Cluster Galaxy in the cluster like typical radio mini-halos. However the total extent of it is 550×800 kpc², which is larger than mini-halos and similar to that of radio halos. The BCG itself is also a radio source with a marginally resolved core at $7''$ (30 kpc) resolution. We measure the 606 MHz flux density of the RH to be 52 ± 5 mJy. Assuming a spectral index of 1.3, the 1.4 GHz radio power is 4.5×10^{24} W Hz⁻¹. The dynamical state of the cluster has been inferred to be "relaxed" and also as "complex" depending on the classification methods based on the morphology of the X-ray surface brightness. This system thus seems to be in the transition phase from a mini-halo to a radio halo.

Key words: acceleration of particles – radiation mechanisms:non-thermal – galaxies:clusters:individual:RXCJ0232.2-4420 – galaxies:clusters:intra-cluster medium – radio continuum:galaxies – X-rays:galaxies:clusters

1 INTRODUCTION

The origin and evolution of cosmic rays and magnetic fields in galaxy clusters is a long standing puzzle. Diffuse radio emission on cluster-wide scales (megaparsec) associated with the intra-cluster medium (ICM) and not with individual galaxies are direct probes of these components. These are typically classified into three classes: radio halos, radio relics and mini-halos (Brunetti & Jones 2014). Radio relics are believed to be direct tracers of cluster merger shocks and observational evidence (e. g. van Weeren et al. 2010; Kale et al. 2012; Stroe et al. 2014) strongly supports this idea though the details of the acceleration mechanism are still under debate (e. g. Brunetti & Jones 2014; Guo et al. 2014).

Radio halos and mini-halos nearly circular in morphology and located co-spatially with the X-ray emission from the ICM (e. g. Feretti et al. 2012; Brunetti & Jones 2014). Mini-halos are 100 - 300 kpc in size and are found in cool-core clusters (e. g. Giacintucci et al. 2017). They are always found to surround the Brightest Cluster Galaxy (BCG). Radio halos are much more extended and can reach sizes of

1- 2 Mpc (Brunetti & Jones 2014). These have been found with higher probability in massive and merging clusters (Cassano et al. 2013).

A component of the relativistic electron population that powers mini-halos and radio halos comes from the hadronic collisions in the ICM (e. g. Dennison 1980; Brunetti et al. 2001; Gitti et al. 2004; Keshet & Loeb 2010). For radio halos it has been found that this component alone is not sufficient and an additional form of turbulent re-acceleration is required (Donnert et al. 2010; Brunetti et al. 2012). Cluster mergers are a natural origin for the turbulence involved and thus the turbulent re-acceleration model can explain the high occurrence of radio halos in massive and merging clusters (e. g. Schlickeiser et al. 1987; Brunetti et al. 2001; Cassano et al. 2013). The mini-halos on the other hand could either be exclusively of hadronic origin or may need turbulence driven by sloshing of sub-clusters or minor mergers (Gitti et al. 2004; ZuHone et al. 2014; Mazzotta & Giacintucci 2008; Giacintucci et al. 2014a; Jacob & Pfrommer 2017; Giacintucci et al. 2017).

Although the radio halos and mini-halos are known to occur in merging and relaxed clusters, respectively, there are systems which are intermediate in their merging sta-

[★] E-mail: ruta@ncra.tifr.res.in

Table 1. Properties of RXCJ0232.2-4420 . Notes: † Bleem et al. (2015, and references therein.) *Laganá et al. (2013)

RA(J2000)(h m s)	02 32 18.7
DEC(J2000) (° ′ ″)	-44 20 41
Redshift (z)	0.2836 [†]
$L_{X[0.1-2.4\text{keV}]}$ (erg s ⁻¹)	13.3×10^{44}
$M_{500}(10^{14} M_{\odot})$	$12.01 \pm 1.80^{\dagger}$
kT(keV)	$8 \pm 1.4^*$
<hr/>	
Radio halo	
Size	550×800 kpc ²
$S_{606\text{MHz}}$	52 ± 5 mJy
$P_{1.4\text{GHz}}$	4.5×10^{24} W Hz ⁻¹

tus. It has been discussed that a transition from a mini-halo to a radio halo triggered by a merger is a possibility (Brunetti & Jones 2014; van Weeren et al. 2019). The transition can also mark the change from a hadronically dominated source to that dominated by turbulent re-acceleration.

In this letter we report the detection of a diffuse radio source which has the properties of mini-halos and also of radio halos that is hosted by the cluster RXCJ0232.2-4420 (Table 1). This cluster was discovered in the ROSAT all sky survey (Craddock et al. 2002) and is known to contain two brightest cluster galaxies (BCGs) separated by 100 kpc (Pierini et al. 2008). It is part of the Archive of Chandra Cluster Entropy Profile Tables (ACCEPT) sample (Cavagnolo et al. 2009) and they report a central entropy (K_0) of 44.62 ± 12.42 keV cm² for this cluster.

We assume a Λ CDM cosmology with $H_0 = 71$ km s⁻¹ Mpc⁻¹, $\Omega_M = 0.27$ and $\Omega_{\Lambda} = 0.73$. This implies a scale of 4.24 kpc arcsec⁻¹ at the redshift 0.2836 of RXCJ0232.2-4420 . The luminosity distance is $D_L = 1444$ Mpc.

2 OBSERVATIONS AND DATA REDUCTION

We have observed cluster RXCJ0232.2-4420 using the GMRT at 610 MHz with 33 MHz bandwidth under observation cycle 31 on 18-Feb-2017 (31_065 PI R. Kale). The cluster was observed for 6 hours with the integration time of 16.10 s. The data were recorded in 256 frequency channels. We used NRAO's Common Astronomy Software Applications (CASA) package for data analysis. A semi-automated pipeline was written for the analysis in python that utilised CASA tasks. The standard steps of flagging (removal of bad data), calibration of complex gains and bandpass were carried out. The flux scale of Perley-Butler 2017 was used for absolute flux calibration. Several rounds of phase only self-calibration followed by amplitude and phase self-calibration were carried out to improve the sensitivity. We imaged the final visibilities with the weighting scheme "briggs" (Briggs 1995) with robust = 0. We imaged the discrete sources using the uv-distance cut of > 5 k λ and subtracted them from the visibilities. A low resolution image of the diffuse source using the uv-distance cut of < 10 k λ was produced. It was convolved to a circular beam of $20'' \times 20''$ for further analysis. The primary beam correction was applied to all the images that were used in the analysis.

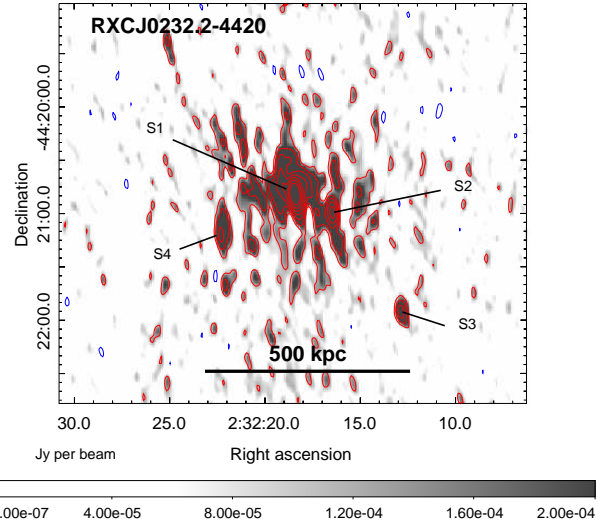


Figure 1. The GMRT 606 MHz image with a resolution of $9.2'' \times 3.9''$, position angle (p. a.) 6.3° and rms of $40 \mu\text{Jy beam}^{-1}$ is shown in grey-scale ($0.1 - 500 \mu\text{Jy beam}^{-1}$) and in contours. The red contours are positive and blue are negative. The contours levels are $\pm 0.12, 0.24, 0.48, 0.96, \dots$ mJy beam⁻¹. The discrete sources S1 - S4 are labelled.

3 RESULTS

The GMRT 606 MHz image with robust=0 weighting of the visibilities is shown in Fig. 1. It has an rms noise of 0.04 mJy beam⁻¹. The discrete radio sources in the field within two arcminutes around the centre are labelled as S1, S2, S3 and S4. The source S1 is associated with the BCG-A in the cluster and shows an extension towards northwest; it is unclear at this resolution if it is a jet (Fig. 2). The source S4 is marginally resolved and does not show association with any galaxy. The sources S2 and S3 are unresolved. The 606 MHz flux densities and the sources within the beam found from the NASA Extragalactic Database (NED) that are the most likely counterparts of these discrete radio sources are given in Table 2.

We have discovered extended diffuse radio emission surrounding the BCG-A in this cluster. Based on the location surrounding the BCG at the peak of X-ray emission from the ICM it looks like a typical mini-halo. However the largest extent of this emission is 800 kpc which is nearly that of giant radio halos ($\gtrsim 700$ kpc, (Cassano et al. 2013)). We refer to this radio emission as a radio halo (RH). The RH is roundish at the centre and shows an extension to the south-east (Fig. 3).

The RH has a flux density of 52 ± 5.0 mJy at 606 MHz ($S_{606\text{MHz}}$) as measured within the area covered by the contour at $3\sigma = 0.3$ mJy beam⁻¹ in the low resolution ($20''$) image. The error on the flux density was calculated according to $\sqrt{(\sigma\sqrt{N_b})^2 + (\sigma_{\text{abs}}S_{606\text{MHz}})^2}$, where N_b is the number of beams in the extent of the emission, σ_{abs} is the percentage error on the absolute flux density scale. We used $\sigma_{\text{abs}} = 0.1$ (e. g. Kale & Parekh 2016) and found $N_b = 75.6$ to get the error of 5 mJy on the 606 MHz flux density of the RH. The K-corrected radio power at frequency ν is

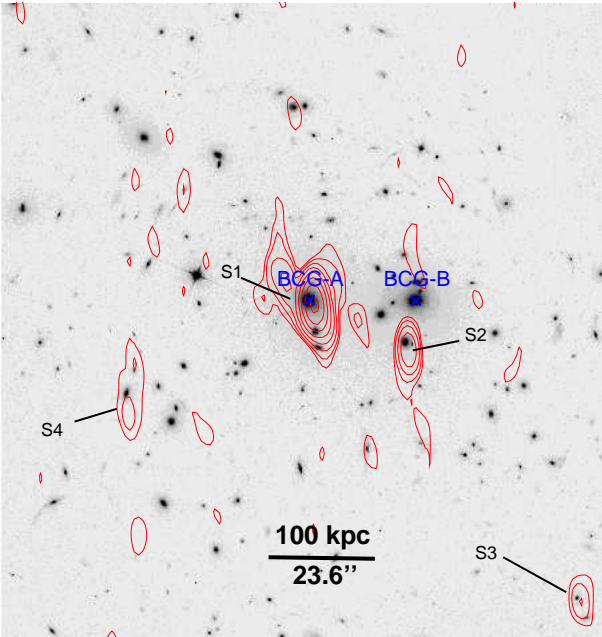


Figure 2. The Hubble Space Telescope WFC3 image with the filter F160W is shown in grey-scale with the contours from the GMRT 606 MHz image using baselines longer than $5k\lambda$. The contours are at 0.15, 0.3, 0.6, ... mJy beam $^{-1}$. The beam is $7.7'' \times 3.4''$, position angle (p. a.) 5° . The discrete sources S1 - S4 are labelled and the positions of BCGs, A and B are marked with crosses.

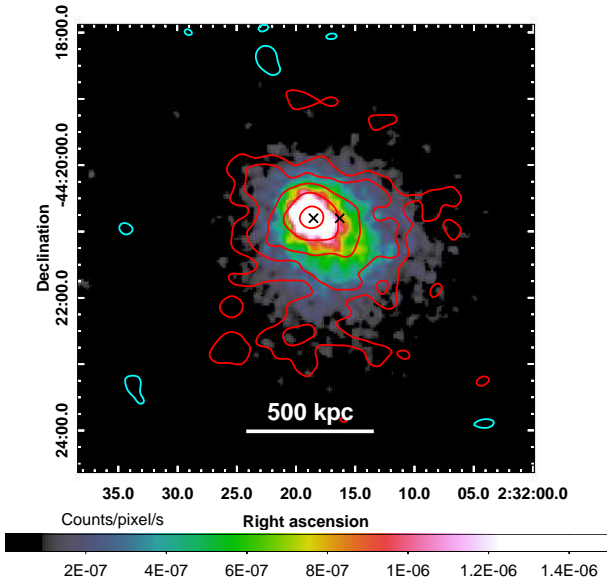


Figure 3. The colour scale shows the Chandra (ObsID 4993) 0.5 - 7 keV image with the contours of radio emission at 606 MHz overlaid. The colour scale range is $1 \times 10^{-9} - 1.5 \times 10^{-6}$ counts pixel $^{-1}$ s $^{-1}$. The pixel size is $1.97''$. The GMRT 606 MHz image with a resolution of $20'' \times 20''$ and rms of 0.1 mJy beam $^{-1}$. The contour levels are $\pm 0.3, 0.6, 1.2, \dots$ mJy beam $^{-1}$. The red contours are positive and cyan are negative. The BCG A and B positions are marked with crosses.

given by, $P_\nu = (4\pi D_L^2) S_\nu (1+z)^{(\alpha-1)}$, where D_L is the luminosity distance. The 606 MHz radio power of the RH is $P_{606\text{MHz}} = 13.9 \pm 1.2 \times 10^{24}$ W Hz $^{-1}$. Assuming a spectral index of 1.3 that is typical for radio halos (Brunetti & Jones 2014) we obtain 1.4 GHz radio power of the RH to be, 4.6×10^{24} W Hz $^{-1}$.

The spectral indices of the diffuse source and that of the BCG could not be determined definitively. We found Sydney University Molonglo Sky Survey 843 MHz image (SUMSS, Mauch et al. 2003), Murchison Widefield Array (MWA) GaLactic and Extragalactic All-sky MWA survey 50 - 200 MHz (GLEAM Wayth et al. 2015) and TIFR GMRT Sky Survey Alternative Data Release 150 MHz (TGSS-ADR Intema et al. 2017) images of this region. The TGSS-ADR 147.5 MHz image had a resolution of $57'' \times 25''$, position angle 0° and the flux density using JMFIT over the source detected around the centre of the cluster is 295 ± 10 mJy. The GLEAM catalogue flux densities of the source J023218-442052 are 228 ± 14 mJy at 223-231 MHz and 1498 ± 67 mJy at 72-80 MHz. These imply a spectral index of 1.7. The GLEAM beam is $134.7'' \times 131.6''$, position angle -30° at 200 MHz and thus cannot resolve the sources S1-S4. The SUMSS catalogue flux density of the central source at 843 MHz is 50.0 ± 3.1 mJy (Mauch et al. 2008). Between SUMSS and TGSS-ADR the spectral index is 1.0. The steeper spectrum within the GLEAM bands may be contribution from the RH. However images with better resolution are needed to separate the discrete and the diffuse emission to determine the spectral index of the diffuse emission.

4 DISCUSSION

4.1 Dynamical state of RXCJ0232.2-4420

In the context of the origin of the diffuse radio emission, the dynamical state of the cluster is important. Lovisari et al. (2017) have carried out a detailed X-ray morphology analysis of a large sample (189) of clusters, including RXCJ0232.2-4420 using XMM-Newton images. Among eight different parameters that they calculate to infer the dynamical state of the cluster, they conclude that centroid shift (w) and concentration (c) are the best estimators of dynamical state. The $w - c$ plane is shown in Fig. 4 for their sample where RXCJ0232.2-4420 is classified as a "relaxed" cluster. In the Archive of Chandra Cluster Entropy Profile Tables (ACCEPT¹) (Cavagnolo et al. 2009), the central temperature of RXCJ0232.2-4420 is reported to be 5.71 ± 0.77 keV and the central cooling time to be 1.38 ± 0.19 Gyr. This central cooling time is consistent with a "weak" cool-core cluster (e. g. Hudson et al. 2010). According to the classification criteria based on central gas density used in Planck Collaboration et al. (2011), this cluster has been classified as a "cool-core" cluster. Thus the properties of the core show evidence of cooling. Weißmann et al. (2013) have discussed morphological classification of galaxy clusters based on the power ratios (P_3/P_0) and centroid shifts (w) using observations with the XMM Newton for a sample 80 clusters that includes RXCJ0232.2-4420. This cluster is classified as "complex" which in their definition is a cluster

¹ <https://web.pa.msu.edu/astro/MC2/accept/>

Table 2. Radio sources in the RXCJ0232.2-4420 field.

Label	RA	Dec	$S_{606\text{MHz}}$ mJy	Identification
S1	02h32m18.421s	-44d20m49.15s	28.05 ± 0.71	2MASS J02321857-4420482 GALEXASC J023218.4-442047.1
S2	02h32m16.471s	-44d20m59.53s	2.67 ± 0.21	2MASS J0231666-4420570
S3	02h32m12.854s	-44d21m55.31s	0.89 ± 0.08	MRSS246-016797 CXOGBAJ023212.9-442154 GALEXASCJ023212.98-442153.9
S4	02h32m22.235s	-44d21m09.36s	1.74 ± 0.20	-

that does not have two maxima in the X-ray surface brightness but has a complex global structure. Thus the works discussed above do not categorise this cluster to be a major merger but do indicate the presence of departure from strong cool-core clusters. The presence of two BCGs in the cluster further indicates a merger in the past.

4.2 Mini-halo to radio halo transition system

The populations of clusters hosting giant radio halos and mini-halos are distinct in their dynamical properties (e.g. Cassano et al. 2010; Kale et al. 2015). It has been proposed that a cool-core cluster with a mini-halo may transition into a radio halo cluster if it undergoes a merger (Brunetti & Jones 2014). While mini-halos could have significant emission due to relativistic electrons that are byproducts of hadronic collisions (Zandanel et al. 2014), a merger can trigger transport of the electrons and turbulent re-acceleration in the outskirts leading to the formation of a radio halo (Brunetti & Jones 2014; van Weeren et al. 2019). The morphology of the RH is nearly symmetric about the BCG-A and shows a southern extension that could be following a sloshing cold-front as found in the case of the mini-halo RX J1720.1 + 2638 (Giacintucci et al. 2014b).

Giacintucci et al. (2017) have studied the distribution of central entropies (K_0) in galaxy clusters with mini-halos and radio halos. They found that the clusters hosting mini-halos have $K_0 < 20 \text{ keV cm}^2$ and those hosting radio halos typically have $K_0 > 50 \text{ keV cm}^2$. With the $K_0 = 44.62 \pm 12.42 \text{ keV cm}^2$, this cluster is in the intermediate zone of radio halos and mini-halos. This is further evidence of it being a transition system. We compared the radio power of RH with that of the mini-halos and radio halos in the $P_{1.4\text{GHz}} - M_{500}$ plane (Fig. 5). The RH radio power is well within the typical powers of radio halos as is also the case for a few other mini-halos. It is among the highest mass clusters hosting mini-halos.

The diffuse radio sources in the clusters Abell 2142, Abell 2390, Abell 2261 and CL1821 + 643 have been classified as peculiar Mpc sized radio sources in cool-core clusters. A two component radio halo is reported in Abell 2142 and is thus unlike typical mini-halos (Venturi et al. 2017). The systems Abell 2390, Abell 2261 (Sommer & Basu 2014) and CL1821 + 643 (Bonafede et al. 2014; Kale & Parekh 2016) are similar to the radio halo reported here. Recently low brightness and steep spectrum emission has been found surrounding the known mini-halos in the clusters PSZ1G139.61+24.20 (Savini et al. 2018) and RXJ1720.1+2638 (Savini et al. 2019). It has been suggested

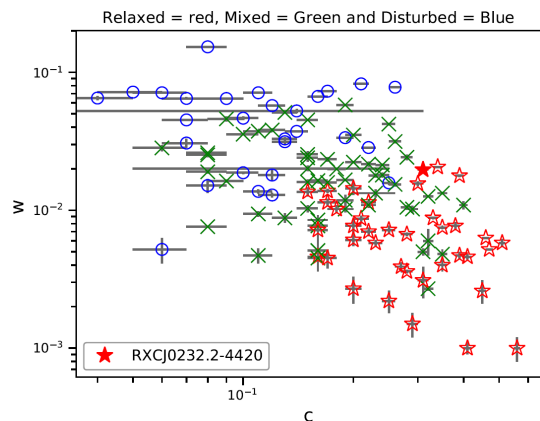


Figure 4. The centroid shift (w) versus concentration (c) parameter plotted for the sample of clusters presented by (Lovisari et al. 2017). The cluster RXCJ0232.2-4420 is in their sample and is highlighted with a filled star symbol. It has been classified as a relaxed cluster according to their classification scheme.

by the authors that sloshing may result in triggering acceleration on large scales. We await our Upgraded GMRT observations to find the spectral index distribution across the radio halo in RXCJ0232.2-4420 and further analysis of the X-ray data to shed more light on the origin of the radio halo.

5 CONCLUSIONS

We report the discovery of diffuse radio emission of size $550 \times 800 \text{ kpc}^2$ surrounding the primary BCG in the cluster RXCJ0232.2-4420 using 606 MHz observations from the GMRT. The 606 MHz flux density of the diffuse radio source is $52 \pm 5 \text{ mJy}$. The diffuse source on one hand is similar to mini-halos in cool-core clusters that surround a BCG and on the other has an extent typical of radio halos. The dynamical state of the cluster based on the X-ray morphology has been termed as "relaxed" and complex making it a transition system between a merger and a cool-core. The 1.4 GHz radio power of the RH is $4.6 \times 10^{24} \text{ W Hz}^{-1}$ assuming a spectral index of 1.3. In the $P_{1.4\text{GHz}} - M_{500}$ plane, it falls within the general trend of the radio halos. Mini-halos are more scattered in this plane and if classified as a mini-halo, it will be the second most massive cluster to host it. The RH properties support the scenario that it is rare system where a mini-halo is transitioning into a radio halo.

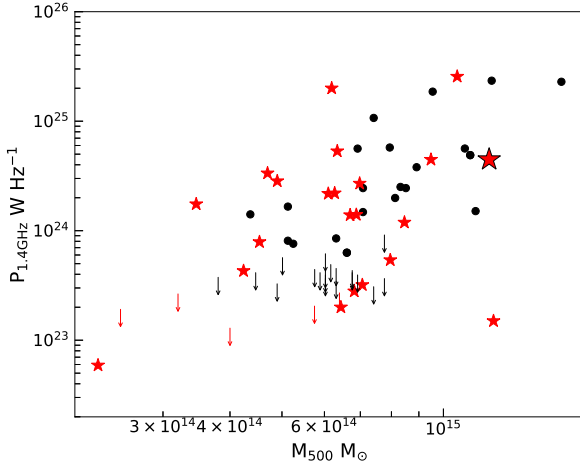


Figure 5. The radio halos (black dots) from Cassano et al. (2013) and mini-halos (small red stars) from Giacintucci et al. (2014a) are plotted in the $P_{1.4\text{GHz}} - M_{500}$ plane. The radio halo upper limits are shown as black arrows and mini-halo upper limits are shown as red arrows (Kale et al. 2015). The big red star symbol marks RXCJ0232.2-4420 .

ACKNOWLEDGEMENTS

We thank the referee for their comments that improved the clarity of the paper. RK acknowledges support through the DST-INSPIRE Faculty Award by the Government of India. We thank the staff of the GMRT that made these observations possible. GMRT is run by the National Centre for Radio Astrophysics of the Tata Institute of Fundamental Research. Based on observations made with the NASA/ESA Hubble Space Telescope, and obtained from the Hubble Legacy Archive, which is a collaboration between the Space Telescope Science Institute (STScI/NASA), the Space Telescope European Coordinating Facility (ST-ECF/ESA) and the Canadian Astronomy Data Centre (CADC/NRC/CSA). This research has made use of the NASA/IPAC Extragalactic Database (NED) which is operated by the Jet Propulsion Laboratory, California Institute of Technology, under contract with the National Aeronautics and Space Administration. This research made use of Astropy, a community-developed core Python package for Astronomy (Astropy Collaboration, 2018). The scientific results reported in this article are based in part on data obtained from the Chandra Data Archive.

REFERENCES

Bleem L. E., et al., 2015, *The Astrophysical Journal Supplement Series*, **216**, 27
 Bonafede A., et al., 2014, *MNRAS*, **444**, L44
 Briggs D. S., 1995, in *American Astronomical Society Meeting Abstracts*. p. 1444
 Brunetti G., Jones T. W., 2014, *International Journal of Modern Physics D*, **23**, 30007
 Brunetti G., Setti G., Feretti L., Giovannini G., 2001, *MNRAS*, **320**, 365
 Brunetti G., Blasi P., Reimer O., Rudnick L., Bonafede A., Brown S., 2012, *MNRAS*, **426**, 956
 Cassano R., Etori S., Giacintucci S., Brunetti G., Markevitch M., Venturi T., Gitti M., 2010, *ApJ*, **721**, L82

Cassano R., et al., 2013, *ApJ*, **777**, 141
 Cavagnolo K. W., Donahue M., Voit G. M., Sun M., 2009, *ApJS*, **182**, 12
 Cruddace R., et al., 2002, *The Astrophysical Journal Supplement Series*, **140**, 239
 Dennison B., 1980, *ApJ*, **239**, L93
 Donnert J., Dolag K., Brunetti G., Cassano R., Bonafede A., 2010, *MNRAS*, **401**, 47
 Feretti L., Giovannini G., Govoni F., Murgia M., 2012, *A&P*, **20**, 54
 Giacintucci S., Markevitch M., Venturi T., Clarke T. E., Cassano R., Mazzotta P., 2014a, *ApJ*, **781**, 9
 Giacintucci S., Markevitch M., Brunetti G., Zuhone J. A., Venturi T., Mazzotta P., Bourdin H., 2014b, *ApJ*, **795**, 73
 Giacintucci S., Markevitch M., Cassano R., Venturi T., Clarke T. E., Brunetti G., 2017, *ApJ*, **841**, 71
 Gitti M., Brunetti G., Feretti L., Setti G., 2004, *A&A*, **417**, 1
 Guo X., Sironi L., Narayan R., 2014, *ApJ*, **797**, 47
 Hudson D. S., Mittal R., Reiprich T. H., Nulsen P. E. J., Anderson H., Sarazin C. L., 2010, *A&A*, **513**, A37
 Intema H. T., Jagannathan P., Mooley K. P., Frail D. A., 2017, *A&A*, **598**, A78
 Jacob S., Pfrommer C., 2017, *MNRAS*, **467**, 1478
 Kale R., Parekh V., 2016, *MNRAS*, **459**, 2940
 Kale R., Dwarakanath K. S., Bagchi J., Paul S., 2012, *MNRAS*, **426**, 1204
 Kale R., et al., 2015, *A&A*, **579**, A92
 Keshet U., Loeb A., 2010, *ApJ*, **722**, 737
 Laganá T. F., Martinet N., Durret F., Lima Neto G. B., Maughan B., Zhang Y. Y., 2013, *A&A*, **555**, A66
 Lovisari L., et al., 2017, *ApJ*, **846**, 51
 Mauch T., Murphy T., Buttery H. J., Curran J., Hunstead R. W., Pietrzynski B., Robertson J. G., Sadler E. M., 2003, *MNRAS*, **342**, 1117
 Mauch T., Murphy T., Buttery H. J., Curran J., Hunstead R. W., Pietrzynski B., Robertson J. G., Sadler E. M., 2008, *VizieR Online Data Catalog*, **8081**
 Mazzotta P., Giacintucci S., 2008, *ApJ*, **675**, L9
 Pierini D., Zibetti S., Braglia F., Böhringer H., Finoguenov A., Lynam P. D., Zhang Y.-Y., 2008, *A&A*, **483**, 727
 Planck Collaboration et al., 2011, *A&A*, **536**, A11
 Savini F., et al., 2018, *MNRAS*, **478**, 2234
 Savini F., et al., 2019, *A&A*, **622**, A24
 Schlickeiser R., Sievers A., Thiemann H., 1987, *A&A*, **182**, 21
 Sommer M. W., Basu K., 2014, *MNRAS*, **437**, 2163
 Stroe A., Harwood J. J., Hardcastle M. J., Röttgering H. J. A., 2014, *MNRAS*, **445**, 1213
 Venturi T., et al., 2017, *A&A*, **603**, A125
 Wayth R. B., et al., 2015, *Publ. Astron. Soc. Australia*, **32**, e025
 Weißmann A., Böhringer H., Chon G., 2013, *A&A*, **555**, A147
 Zandanel F., Pfrommer C., Prada F., 2014, *MNRAS*, **438**, 124
 Zuhone J., Brunetti G., Giacintucci S., Markevitch M., 2014, preprint, ([arXiv:1403.6743](https://arxiv.org/abs/1403.6743))
 van Weeren R. J., Röttgering H. J. A., Brüggén M., Hoeft M., 2010, *Science*, **330**, 347
 van Weeren R. J., de Gasperin F., Akamatsu H., Brüggén M., Feretti L., Kang H., Stroe A., Zandanel F., 2019, arXiv e-prints,

This paper has been typeset from a $\text{\TeX}/\text{\LaTeX}$ file prepared by the author.